Electronic Supplementary Material (ESI) for Nanoscale.

Supplementary Material

Oriental and robust anchoring of Fe via anodic interfacial coordination assembly on ultrathin Co hydroxides for efficient water oxidation

Ya-Nan Zhou, Ruo-Yao Fan, Yu-Ning Cao, Hui-Ying Wang, Bin Dong *,

Hui-Ying Zhao, Fu-Li Wang, Jian-Feng Yu, Yong-Ming Chai *

State Key Laboratory of Heavy Oil Processing, College of Science, China University of Petroleum (East China), Qingdao 266580, PR China

*** Corresponding Authors.**

Email: dongbin@upc.edu.cn (B. Dong), ymchai@upc.edu.cn (Y.M. Chai)

Characterization

The morphology and microstructure of all samples were characterized SEM (JEM 2100F) and TEM (FEI Tecni G20, 200 kV). X-ray diffraction (XRD) with Cu Kα radiation (λ = 1.54 Å) on the Brook D8 advance equipment to examine the crystalline structures and phase purity of the samples. Raman spectra was obtained via LabRAM HR Evolution with an excitation wavelength of 514 nm. The element composition and distribute on of the sample were characterized by the Energy Dispersive System (EDS) and inductively coupled plasma mass spectrometry (ICP-MS) detected on the Hitachi S-4800 and Agilent ICPMS7700, respectively. X-ray photoelectron spectroscopy (XPS) was acquired on Thermo Fisher K-alpha 250Xi to quantitatively research the chemical and electronic states of the sample elements.

Electrochemical measurements

Electrochemical tests were performed at room temperature on a standard three-electrode configuration in 1.0 M KOH with Gamry Reference 600 electrochemical equipment. The working electrode was prepared as follows: 4 mg catalyst and 20 μL Nafion solution (5 wt %) were dispersed in 1 mL of water/ethanol solution (v_{water} : $v_{ethanol}$ = 1:1) by sonicating at least 30 min to form a homogeneous ink. Then 5 μL of suspensions were coated on glassy carbon electrode (GCE) with a diameter of 3 mm, and dried in air before measurement. The glassy carbon (GC) electrode loaded catalysts, Pt foil and saturated calomel electrode (SCE) were used as working electrode, counter electrode and reference electrode, respectively. The linear sweep voltammetry (LSV) were detected at same condition with scan rate of 5 mV s^{-1} with iR-correction. All the potentials vs. SCE were converted into a standard reversible hydrogen electrode (RHE) via the Nernst equation: $E_{RHE} = E_{SCE} + 0.0594pH + 0.245$. The electrical

double-layer capacitances (C_{dl}) were calculated by cyclic voltammetry (CV) curves with the scan rate of 40, 60, 80, 100, 120 mV s^{-1}, respectively. And electrochemical impedance spectroscopy (EIS) was performed with the frequency ranges from 10^5 Hz to 0.1 Hz. The stability of the samples was measured through CV curves for 2000 cycles at 40 mV s^{-1} and chronoamperometry at 0.52 V vs. SCE.

Density Functional Theory Calculations

The density functional theory (DFT) calculations were carried out by using the Materials Studio. The exchange–correlation interaction was described by generalized gradient approximation (GGA) with the Perdew-Burke-Ernzerhof (PBE) functional. The energy cutoff was set to 570 eV. The Monkhorst-Pack k-point mesh was set as 9 × 9 × 6 and 8 × 5 × 3 for $Co(OH)_2$ and TF@$Co(OH)_2$ models, respectively. The convergence criterion in geometry optimization was set as 10^{-5} eV/atom for energy.

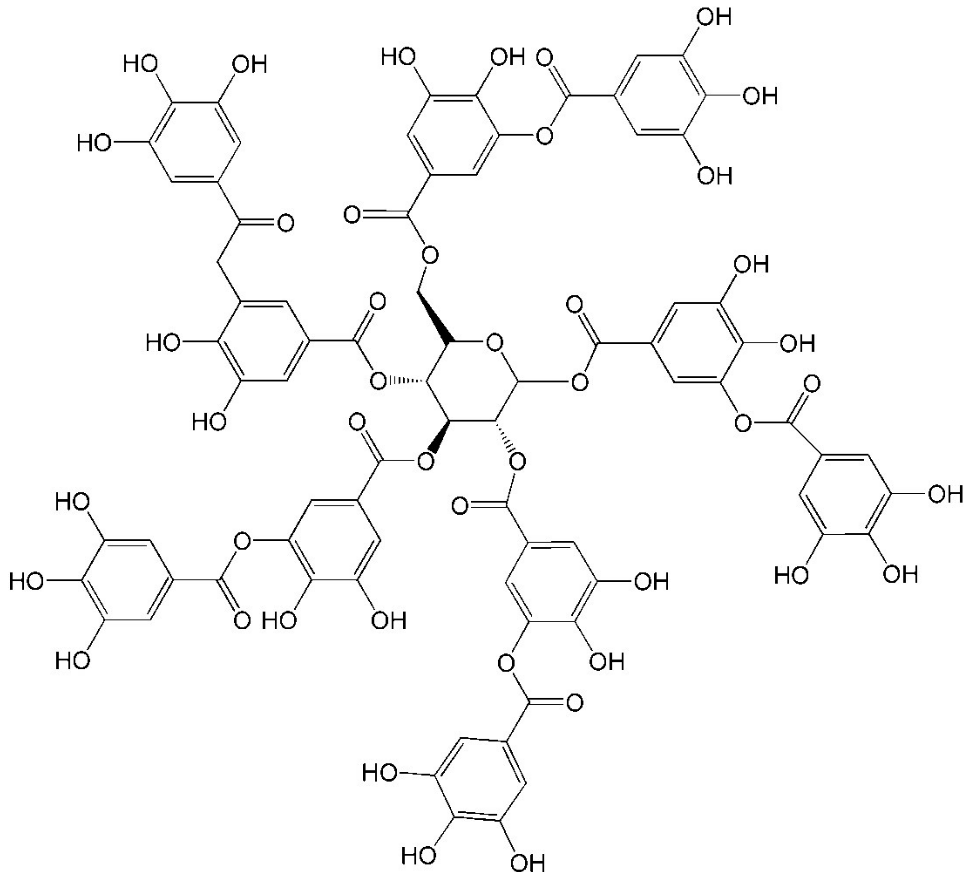

Fig. S1. The molecular structure of tannic acid.

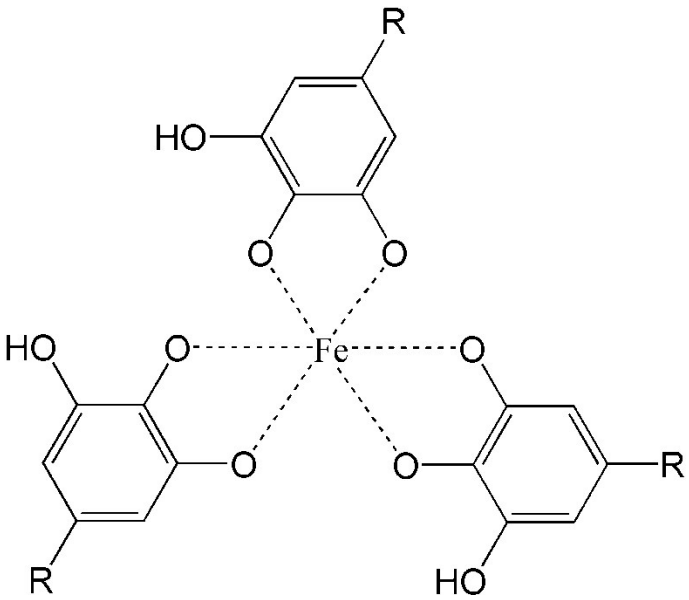

Fig. S2. The dominant complexation state of TA-Fe at pH > 7.

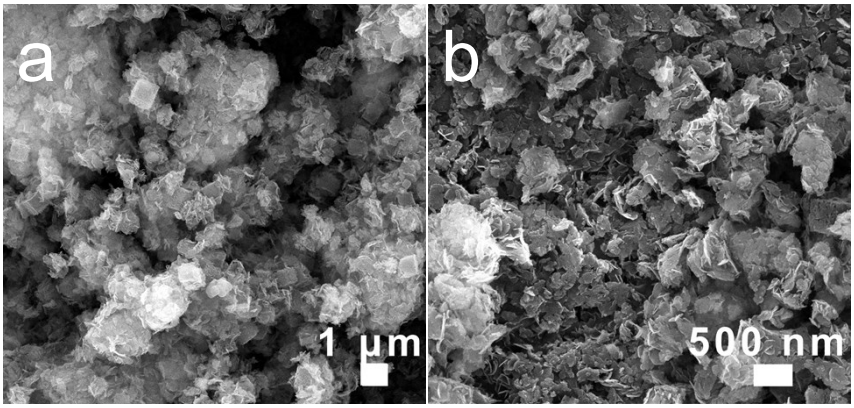

Fig. S3. SEM images of ZIF-67@$Co(OH)_2$.

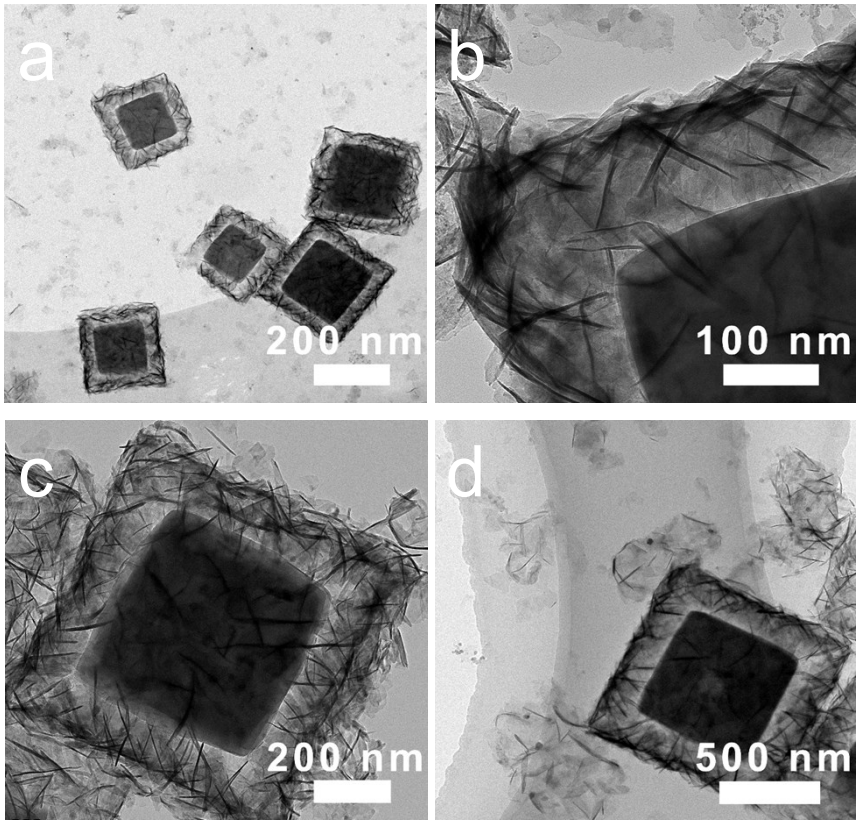

Fig. S4. TEM images of (a,b) ZIF-67@$Co(OH)_2$, (c) Fe@$Co(OH)_2$, (d) TA@$Co(OH)_2$.

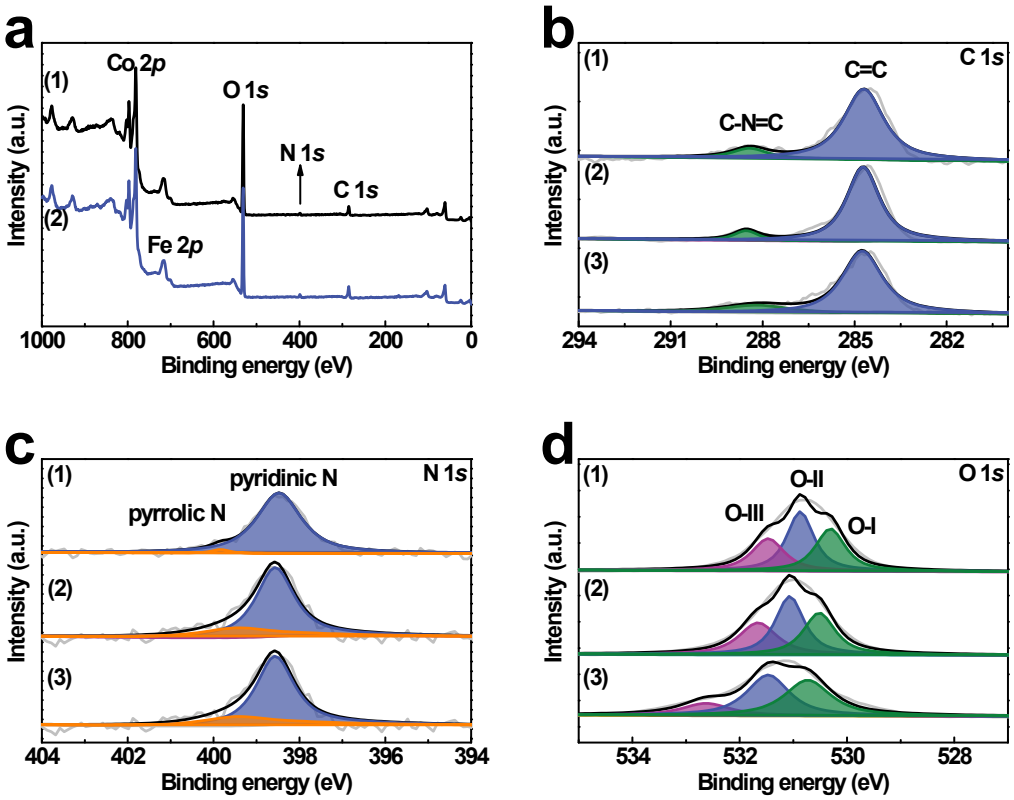

Fig. S5. (a) XPS survey peaks of ZIF-67@$Co(OH)_2$ and TF@$Co(OH)_2$-*t*, The high-resolution scans for ZIF-67@$Co(OH)_2$ and TF@$Co(OH)_2$-*t* in (b) C 1*s*, (c) N 1*s* and (d) O 1*s* regions. The (1) (2) and (3) respectively represent the ZIF-67@$Co(OH)_2$, TF@$Co(OH)_2$-500, and TF@$Co(OH)_2$-1000.

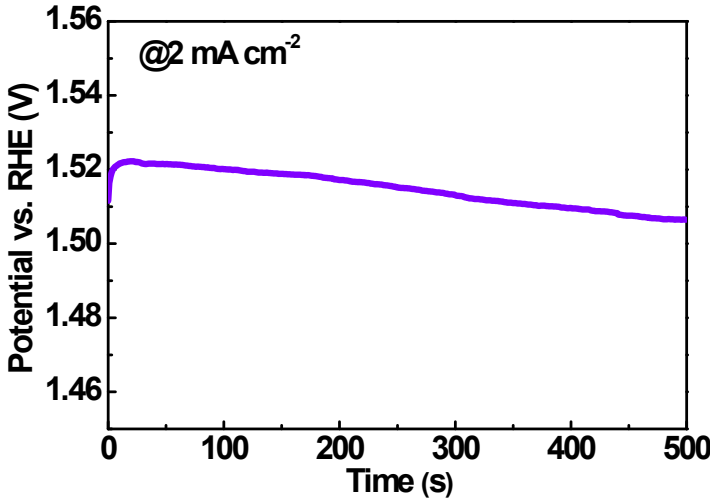

Fig. S6. The chronopotentiometry at 2 mA cm^{-2} of TA-Fe coating.

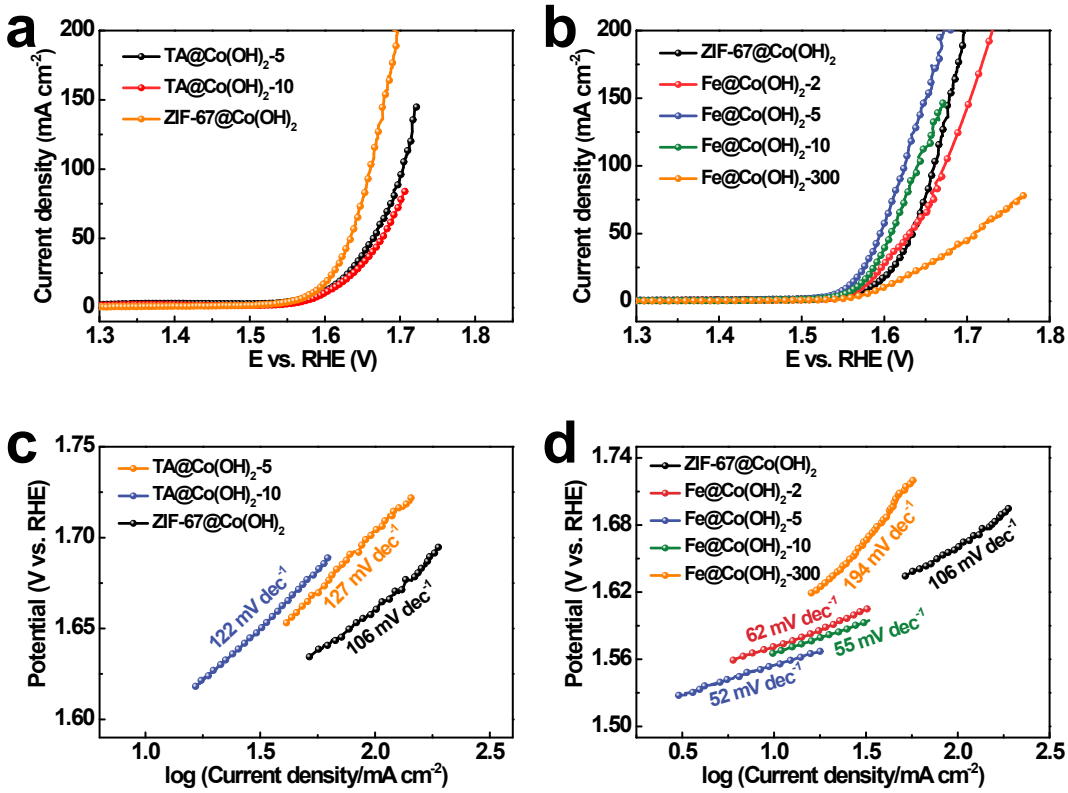

Fig. S7. (a,b) Linear sweep voltammetry curves of various electrocatalysts in 1.0 M KOH solution at a scan rate of 5 mV s^{-1}, (c,d) The corresponding Tafel plots.

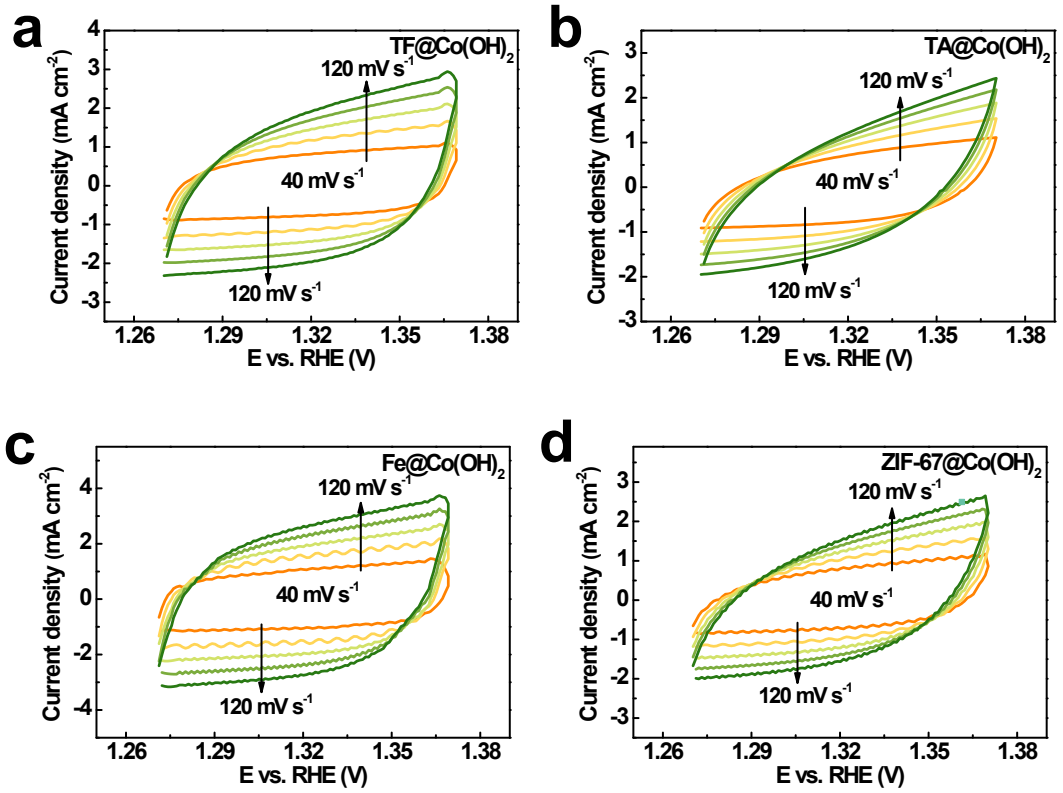

Fig. S8. The cyclic voltammetry curves of $TF@Co(OH)_2$, $TA@Co(OH)_2$, $Fe@Co(OH)_2$ and $ZIF\text{-}67@Co(OH)_2$ in 1.0 M KOH at the scan rate of 40 mV, 60 mV, 80 mV, 100 mV and 120 mV.

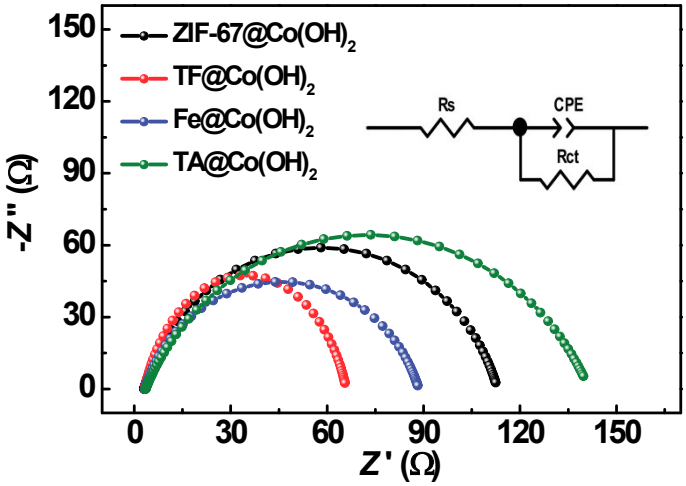

Fig. S9. The Electrochemical impedance spectroscopy curves of TF@$Co(OH)_2$, TA@$Co(OH)_2$, Fe@$Co(OH)_2$ and ZIF-67@$Co(OH)_2$.

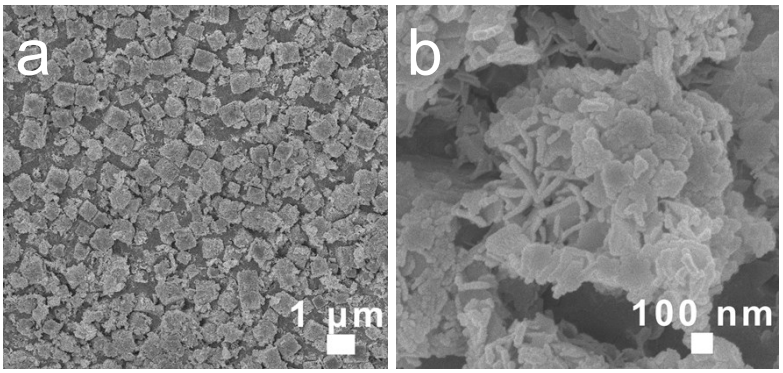

Fig. S10. The morphology of TF@$Co(OH)_2$ after 2000 cycles.

Table S1. The EDS spectrum and corresponding element contents of Co, Fe, C, N, O in TA@$Co(OH)_2$-500.

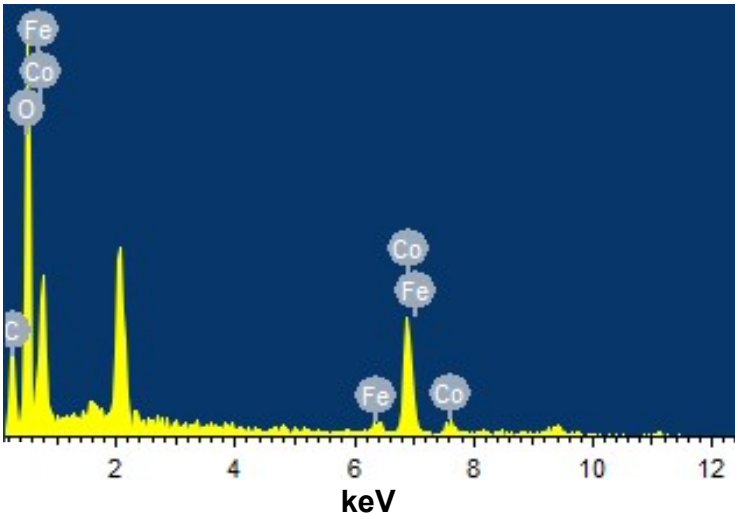

Element	Wt.%	At.%
C K	29.35	48.35
N K	8.66	12.23
O K	20.64	25.52
Fe K	0.49	0.17
Co K	40.86	13.72
Total account	100.00	100.00

Table S2. The EDS spectrum and corresponding element contents of Co, Fe, C, N and O in Fe@$Co(OH)_2$-5.

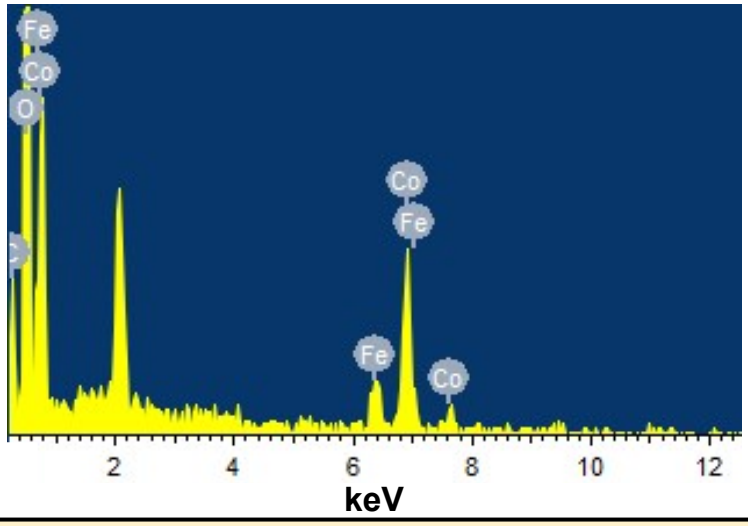

Element	Wt.%	At.%
C K	17.90	33.72
N K	0.32	0.52
O K	33.28	47.06
Fe K	4.38	1.77
Co K	44.11	16.93
Total account	100.00	100.00

Table S3. The EDS spectrum and corresponding element contents of Co, Fe, C, N and O in Fe@$Co(OH)_2$-300.

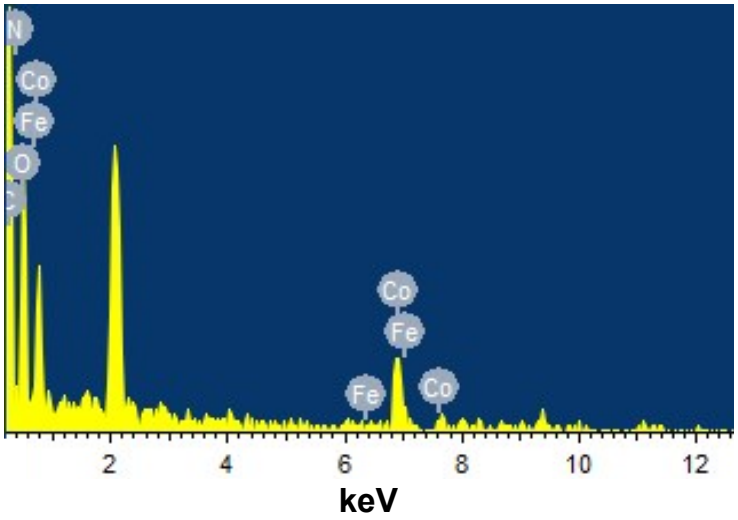

Element	Wt.%	At.%
C K	12.87	22.09
N K	5.59	8.23
O K	43.41	55.93
Fe K	21.84	8.06
Co K	16.28	5.69
Total account	100.00	100.00

Table S4. The atomic ratio of Co^{2+} and Co^{3+} estimated from XPS Co 2*p* spectra.

Sample	The atomic ratio of Co^{2+} and Co^{3+}
ZIF-67@$Co(OH)_2$	1.10
TF@$Co(OH)_2$-500	1.06
TF@$Co(OH)_2$-1000	1.00

Table S5. The atomic ratio of Fe^{2+} and Fe^{3+} estimated from XPS Fe 2*p* spectra.

Sample	The atomic ratio of Fe^{2+} and Fe^{3+}
TF@$Co(OH)_2$-500	0.65
TF@$Co(OH)_2$-1000	0.44

Table S6. ICP content result of KOH (1 M) electrolyte for TF@$Co(OH)_2$-500 and Fe@$Co(OH)_2$ before and after 10 h OER stability in 1.0 M KOH.

	Fe (mg/L)	
Fe@$Co(OH)_2$	Before	After
	0.07	4.70
TF@$Co(OH)_2$-500	Before	After
	0.07	2.21

Table S7. The comparison of OER activity between TF@$Co(OH)_2$-500 and other reported Co-besed electrocatalysts in 1.0 M KOH.

Electrocatalyst	j ($mA\ cm^{-2}$)	η (mV)	b ($mV\ dec^{-1}$)	Ref.
TF@$Co(OH)_2$-500	10	317	47	This work
Fe1Co2-NC	10	356	86.6	[1]
Co/Mo2C@NC-800-2	10	311	131.5	[2]
Co-VN@C	10	330	111.0	[3]
NiCo-BDC	10	343	85	[4]
Co(OH)2-exf	10	390	57	[5]
Fe-Co PBA NPs	10	460	105	[6]
Fe-Co/NPC	10	396	53.55	[7]
K-ZIF-67-Ac	50	350	56.87	[8]
CeO2/$Co(OH)_2$	10	410	66	[9]
Co0.89Ca0.11-CPs	10	371	58.3	[10]
Co/CoO@C	10	320	143	[11]
CFO1	10	304	38	[12]
Co@N-CNTF-2	10	350	61.4	[13]
(Co/Fe)(4)O-4 Cubane	10	300	36	[14]
$Co(OH)_2$@$Ni(OH)_2$	10	330	223	[15]

Reference

[1] Y. Lei, R.X. Huang, H.M. Xie, D.D. Zhang, X.Y. Liu, Y.J. Si, N. Li, Electronic structure tuning of FeCo nanoparticles embedded in multi-dimensional carbon matrix for enhanced bifunctional oxygen electrocatalysis, J. Alloys Compd. 853 (2021) 157070.

[2] G.P. Liu, K.K. Wang, L. Wang, B. Wang, Z.X. Lin, X. Chen, Y.J. Hua, W.S. Zhu, H.M. Li, J.X. Xia, A Janus cobalt nanoparticles and molybdenum carbide decorated N-doped carbon for high-performance overall water splitting, J. Colloid Interface Sci. 583 (2021) 614−625.

[3] T. Peng, Y. Guo, Y.G. Zhang, Y.B. Wang, D.Y. Zhang, Y. Yang, Y. Lu, X.F. Liu, P.K. Chu, Y.S. Luo, Uniform cobalt nanoparticles-decorated biscuit-like VN nanosheets by in situ segregation for Li-ion batteries and oxygen evolution reaction, Appl. Surf. Sci. 536 (2021) 147982.

[4] C. Shuai, Z.L. Mo, X.H. Niu, P. Zhao, Q.B. Dong, Y. Chen, N.J. Liu, R.B. Guo, Nickel/cobalt bimetallic phosphides derived metal-organic frameworks as bifunctional electrocatalyst for oxygen and hydrogen evolution reaction, J. Alloys Compd. 847 (2020) 156514.

[5] N.P. Dileep, T.Z.V.Vineesh, P.V. Sarma, M.V. Chalil, C.S. Prasad, M.M. Shaijumon, Electrochemically exfoliated beta-$Co(OH)_2$ nanostructures for enhanced oxygen evolution electrocatalysis, ACS Appl. Energy Mater. 3 (2020) 1461−1467.

[6] M. Ishizaki, H. Fujii, K.Toshima, H.Tanno, H.Sutoh, M. Kurihara, Preparation of Co-Fe oxides immobilized on carbon paper using water-dispersible Prussian-blue

analog nanoparticles and their oxygen evolution reaction (OER) catalytic activities, Inorg. Chim. Acta, 502 (2020) 119345.

[7] H.X. Jia, M.Z. Zhang, T.J. Meng, S.Y. An, H. Wang, X.J. Yang, Y.F. Zhang, Facile synthesis of Fe, Co bimetal embedded nanoporous carbon polyhedron composites for an efficient oxygen evolution reaction, J. Colloid Interface Sci. 563 (2020) 189−196.

[8] J.L. Chang, Y.F. Wang, L.M. Chen, D.P. Wu, F. Xu, Z.Y. Bai, K. Jian, Z.Y. Gao, Cobalt nanoparticles embedded nitrogen doped carbon, preparation from alkali deprotonation assisted ZIF-67 and its electrocatalytic performance in oxygen evolution reaction, Int. J. Hydrogen Energy, 45 (2020) 12787−12797.

[9] M.C. Sung, G.H. Lee, D.W. Kim, $CeO_2/Co(OH)_2$ hybrid electrocatalysts for efficient hydrogen and oxygen evolution reaction, J. Alloys Compd. 800 (2019) 450−455.

[10] P.P. Su, S.S. Ma, W.J. Huang, Y. Boyjoo, S.Y. Bai, J. Liu, Ca^{2+}-doped ultrathin cobalt hydroxyl oxides derived from coordination polymers as efficient electrocatalysts for the oxidation of water, J. Mater. Chem. A 7 (2019) 19415−19422.

[11] H.Y. Huang, Y.Q. Li, W.B. Li, S.R Chen, C. Wang, M. Cui, T.L Ma, Enhancing oxygen evolution reaction electrocatalytic performance with vanadium-doped Co/CoO encapsulated in carbon nanorod, Inorg. Chem. Commun. 103 (2019) 1−5.

[12] F.L Yu, Y. Bai, Q. Wang, L. Wang, X. Zhang, Y. Yin, Coordination-assisted synthesis of iron-incorporated cobalt oxide nanoplates for enhanced oxygen evolution, Mater. Today Chem. 11 (2019) 112−118.

[13] H.L. Guo, Q.C. Feng, J.X. Zhu, J.S. Xu, Q.Q. Li, S.L. Liu, K.W. Xu, C. Zhang, T.X. Liu, Cobalt nanoparticle-embedded nitrogen-doped carbon/carbon nanotube frameworks derived from a metal-organic framework for tri-functional ORR, OER and HER electrocatalysis, J. Mater. Chem. A 7 (2019) 3664−3672.

[14] J.C. Li, Q.W. Zhou, C.L. Zhong, S.W. Li, Z.H. Shen, J. Pu, J.Y. Liu, Y.M. Zhou, H.G. Zhang, H.X. Ma, (Co/Fe)(4)O-4 cubane-containing nanorings fabricated by phosphorylating cobalt ferrite for highly efficient oxygen evolution reaction, ACS Catal. 9 (2019) 3878−3887.

[15] Y.L. Wang, Y.X. He, M. Zhou, Fabrication of hierarchical $Co(OH)_2$@$Ni(OH)_2$ core-shell nanosheets on carbon cloth as an advanced electrocatalyst for oxygen evolution reaction, Appl. Surf. Sci. 479 (2019) 1270−1276.